Analytical Methods

ROYAL SOCIETY OF CHEMISTRY

PAPER

View Article Online
View Journal

Cite this: DOI: 10.1039/d0ay01163k

Gold nanoparticle-engineered electrochemical aptamer biosensor for ultrasensitive detection of thrombin

Ying Chen,† Junyi Xiang,† Bin Liu, Zhengbo Chen * and Xia Zuo *

In order to obtain a lower detection limit in electrochemical detection, the choice of signal amplification strategy is of great importance. In this work, we describe an electrochemical sandwich aptasensor based on a signal amplification system involving two thrombin (TB) aptamers (TBA1 and TBA2), gold nanoparticles (AuNPs) as aptamer carriers, and $[Ru(NH_3)_6]^{3+}$ for signal conversion. In the presence of the target thrombin, TBA1 and TBA2 specifically bind to TB, and the TBA1–TB–TBA2 complexes cause the formation of a sandwich structure, meaning more $[Ru(NH_3)_6]^{3+}$ can be adsorbed on the negatively charged phosphate backbone of the aptamers, resulting in an increase in the differential pulse voltammetry (DPV) current. Under optimal conditions, the aptasensor exhibited a linear range of 1 fM to 6 pM and a limit of detection of 0.1429 fM (S/N = 3) for TB. The proposed aptasensor displayed an excellent selectivity and reproducibility. Importantly, the aptasensor was capable of detecting TB in serum samples successfully.

Received 12th June 2020
Accepted 3rd July 2020

DOI: 10.1039/d0ay01163k

rsc.li/methods

Introduction

Thrombin (TB) is an allosteric serine protease, which does not exist in the bloodstream under common conditions, and plays a significant role in the coagulation process. When a blood vessel is damaged, the inactive zymogen prothrombin quickly generates TB, which converts soluble fibrinogen into its insoluble counterpart, thereby acting as a coagulant.[1,2] TB serves an increasingly indispensable role in the pathological activities of diseases such as coagulopathy, cancer, and atherosclerosis. Therefore, it is vitally important to specifically detect TB in serum samples and complex environments.[3–5]

Aptamers are usually peptide molecules or oligonucleotides that can bind to a variety of specific targets such as heavy metal ions, proteins, viruses, and even cells.[6–9] Compared with traditional antibodies, aptamers are promising candidates for bioassay applications because of their specificity, easy labeling, cost-effectiveness, small size, and good chemical stability.[10–12] By virtue of these advantages, electrochemical aptasensors show remarkably advantageous properties including a high sensitivity, low detection limit, moderate cost, fast response speed, portability, and ease of operation in the field of sensors.[13,14] Heeger *et al.* reported a set of novel aptamer-based sensors for the detection of multiple target molecules, but the single sensor restricted the signal intensity of detection.[15–17] Xiao *et al.* developed a universal aptamer-based electrochemical sensor to detect thrombin using target-induced strand displacement, but this strategy is deficient in sensitivity as the detectable limit is 3 nM.[18] Fan *et al.* designed a target-response electrochemical aptamer switch (TREAS) with a simple design and versatile signal for the detection of adenosine triphosphate (ATP), nevertheless, the reagentless structure also lacks a strong detection signal.[19] All of the above mentioned electrochemical aptasensors are based on a mechanism in which redox labels are combined with surface-restricted aptamers to induce conformational changes, which provides us with novel ideas of how to develop a highly sensitive biosensor with an amplified electric signal.

In order to further improve the sensitivity of the aptamer-based sensor, an effectual signal amplification strategy was necessary for the detection of a protein at a low concentration.[20,21] Over the past decade, oligonucleotide-functionalized gold nanoparticles (AuNPs) have been widely applied as amplifying tags for novel biosensing schemes because they can easily bind to biomolecules and have an excellent electrochemical performance.[22,23] It has been reported that each gold nanoparticle (AuNP) could be loaded with hundreds of DNA strands.[24,25] Shen *et al.* proposed an electrochemical DNAzyme sensor for the sensitive detection of Pb^{2+}, which utilized the catalytic reaction when the DNAzyme bound to Pb^{2+} and allowed amplification of DNA-Au bio-barcodes, in which $[Ru(NH_3)_6]^{3+}$ was selected as an electrical signal readout.[26]

Based on the above-mentioned studies, herein, we developed an electrochemical sandwich-type aptasensor to detect TB, which is based on the high DNA loading capacity of AuNPs for signal amplification and $[Ru(NH_3)_6]^{3+}$ for signal conversion

Department of Chemistry, Capital Normal University, Beijing, 100048, China. E-mail: czb979216@sina.com; zuoxia@cnu.edu.cn

† These authors contributed to this work equally.

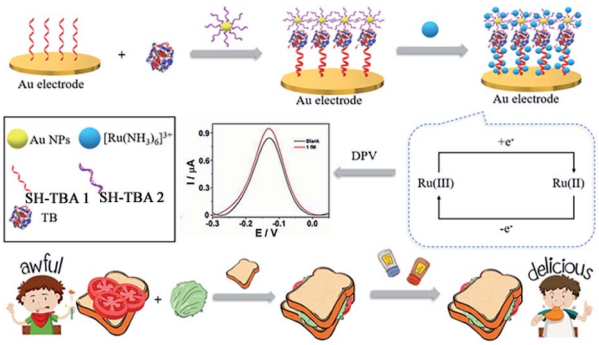

Scheme 1 Schematic diagram of the modification process and sensing mechanism of the electrochemical sensor.

(Scheme 1). First, 13 nm AuNPs were used as a carrier to load a large amount of the thrombin aptamer (TBA2) to form the AuNP–TBA2 conjugates. Second, the other thrombin aptamer 1 (TBA1) was immobilized on the electrode surface by the Au–S bonds. TBA1 and TBA2 could bind TB to form a sandwich structure. $[Ru(NH_3)_6]^{3+}$ was used as a signal converter, this could electrostatically bind to the negatively charged DNA backbone. As a result, the binding of more TB to the electrode surface triggered more AuNP–TBA2 conjugates to be fixed onto the electrode, so that more $[Ru(NH_3)_6]^{3+}$ could be adsorbed onto the aptamers to produce a larger electrical signal. The novelty of this work lies in the double amplification of electrical signals to achieve a higher sensitivity. The double signal amplification is reflected in the following two aspects, AuNPs with a large specific surface area act as a fixed carrier for a large amount of TBA2, and a sandwich structure was formed by the TBA1–TB–TBA2 complexes, therefore many DNA strands can absorb more signal probe molecules ($[Ru(NH_3)_6]^{3+}$).

Experimental

Reagents

Tris(2-carboxyethyl) phosphine hydrochloride (TCEP), hydrogen tetrachloroaurate(III) hydrate ($HAuCl_4$), sodium citrate, hexaammineruthenium(III) chloride, 6-mercaptohexanol (MCH), lysozyme (Lys), pepsin (Pep), papain (Pap), bovine hemoglobin (Hem), bovine serum albumin (BSA), human serum albumin (HSA), and thrombin (TB) were obtained from Sigma-Aldrich. Ultrapure water was used from a Millipore water purification system to prepare the aqueous solution. TB oligonucleotides were synthesized and purified by Sangon Biotech (Beijing, China). The sequence of the oligomer used was as follows:

TBA1: 5′-SH-$(CH_2)_6$-GGT TGG TGT GGT TGG-3′

TBA2: 5′-SH-AGT CCG TGG TAG GGC AGG TTG GGG TGA CT-3′.

Instrumentation

Electrochemical measurements were performed on a CHI650e electrochemical workstation (Chenhua Instruments Co., Shanghai, China). The three-electrode system used consisted of a bare gold electrode (diameter, 2 mm) as the working electrode, a saturated Ag/AgCl electrode as the reference electrode, and a platinum wire as the counter electrode. All characterization of the electrode was performed in 1 mM potassium ferricyanide solution, and all measurements were carried out in a specific buffer (I–B: 20 mM Tris–HCl, pH 7.41 with 140 mM NaCl, 20 mM $MgCl_2$, and 20 mM KCl).

Preparation of AuNP–TBA2

The AuNPs were prepared by reducing $HAuCl_4$ with sodium citrate.[27] Briefly, 100 mL of 1 mM $HAuCl_4$ was first heated to reflux while stirring. Then, 2 mL of 194 mM sodium citrate was added quickly to the vortex of the solution. The color of the solution changed from pale yellow to dark red. After discoloration, this was refluxed for another 20 min and then cooled to room temperature. The UV-vis absorption peak for the AuNP colloids with an average diameter of about 13 nm appeared at about 520 nm, which was consistent with the absorption of the AuNPs of this size.

The AuNP–TBA2 conjugates were prepared according to a previously described literature method.[28] 2.97 mL of AuNP solution (10 nM) was mixed with 30 μL of the TBA2 aqueous solution (100 μM), and this was incubated at 37 °C for 16 h to form the AuNP–TBA2 conjugates.

Sensor preparation

The gold electrode with a diameter of 2 mm was polished with 0.3 μm and 50 nm alumina powder, and then ultrasonically treated with deionized water and ethanol (15 s each time). Afterwards, the electrode was subsequently voltammetrically cycled in 0.5 M H_2SO_4 with a potential between −0.2 and +1.5 V at 0.1 V s^{-1} until a representative cyclic voltammogram of the clean gold electrode was obtained.

The cleaned electrode was immersed for 14 h in a solution consisting of 1 mM TB aptamer (TBA1), a specific buffer (I–B: 50 mM Tris–HCl, pH 7.41 with 140 mM NaCl, 20 mM $MgCl_2$ and 20 mM KCl) and 1 mM TCEP at 37 °C. Then, the surface was passivated with 1 mM MCH for 30 min to obtain a well-aligned monolayer of TBA1. After passivation, the electrode was washed three times with 50 mM Tris–HCl buffer (pH 7.41) and electrochemically characterized in 1 mM potassium ferricyanide solution. Prior to TB binding, the electrode was incubated with 50 mM $[Ru(NH_3)_6]^{3+}$ for 5 min to allow $[Ru(NH_3)_6]^{3+}$ to bind to the TBA1 through the negatively charged phosphate backbone and to ensure that the TBA-modified surface was saturated with the redox-active complex. The total amount of TBA immobilized on the gold electrode surface was 3×10^{10} molecules. In order to detect TB, 10 μL TB standard solution diluted with AuNP–TBA2 conjugates was deposited onto the gold electrode modified with TBA1 for incubation for 12 h.

Results and discussion

Principle of the aptasensor

In Scheme 1, the principle and gradual modification process of the electrochemical sensor for thrombin detection are described. First, TBA1 was immobilized on the surface of the activated bare

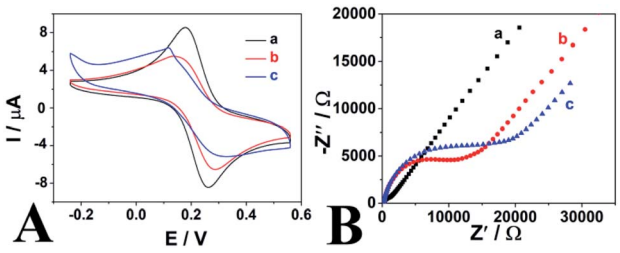

Fig. 1 CV (A) and EIS (B) of the different modified electrodes in 1 mM $[Fe(CN)_6]^{3-/4-}$ at the bare gold electrode (a), TBA1/GE (b), and the AuNPs/TBA2/10 fM TB/TBA1/gold electrode (c).

gold electrode *via* Au–S bonds to capture the target molecule TB. SH-TBA2 was fixed onto the AuNP surface to construct the AuNPs–TBA2 probe. In the presence of TB, TBA1 and TBA2 could be combined with TB and folded into a complex structure similar to a "sandwich" at the electrode. Secondly, it was ensured that the aptamer-modified electrode was fully exposed to the hexaammineruthenium(III) chloride aqueous solution. The $[Ru(NH_3)_6]^{3+}$ was bound to the anionic DNA backbone through electrostatic attraction, and as a signal converter, it can undergo redox reactions on the electrode to produce electrical signals.[29] As a result, with the increase in the TB concentration, there were more AuNPs–TBA2 probes attached to the electrode, thus a growing amount of $[Ru(NH_3)_6]^{3+}$ was adsorbed onto the DNA chain, giving rise to a significantly stronger electrical signal.

Characterization of the electrochemical sensor

The step-wise modification of the electrochemical sensor was characterized using cyclic voltammetry (CV) measurements (Fig. 1A). Owing to the poor conductivity of the TBA1 layer and the electrostatic repulsion between the electronegative DNA and redox species ($[Fe(CN)_6]^{3-/4-}$), the TBA1 modified electrode (curve b) shows a reduced current response compared to the bare gold electrode (curve a). After incubation with AuNPs–TBA2 (curve c), a lower current response was generated because more TBA2 was connected to the electrode. Electrochemical impedance spectroscopy (EIS) measurements (Fig. 1B) were also used to monitor the fabrication process of the electrochemical sensor. In the Nyquist diagram, the charge transfer resistance is proportional to the diameter of the semicircle. As shown in Fig. 1B, compared with the bare gold electrode (curve a), the TBA1-modified electrode (curve b) had a larger semicircle, indicating that the incubated TBA1 weakened the conductivity of the sensing interface. As the electrode was further modified by AuNPs–TBA2 (curve c), the semicircle radius became larger, indicating that the charge transfer resistance of the electrode had further increased. These CV and EIS measurements prove that the electrochemical sensor was successful established.

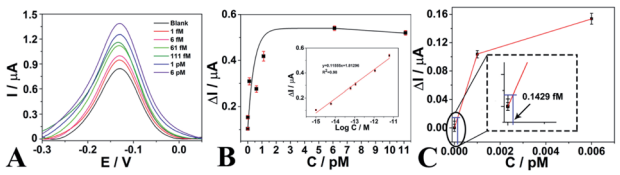

Fig. 2 (A) DPV responses of the electrochemical sensor towards different concentrations of TB (0–6 fM) in 0.05 M Tris–HCl buffer (pH = 7.4) containing 50 mM $[Ru(NH_3)_6]^{3+}$. (B) Calibration curve between the DPV current values and different concentrations of TB. Inset shows the established standard curves between the DPV current values and the logarithm of the TB concentrations. (C) The detection limit for TB according to the 3σ rule.

Performance of the aptasensor for TB detection

When TB was present, the specificity between the aptamers and TB enabled the connection of AuNPs–TBA2 to the TBA1-modified Au electrode, resulting in an increase in the amount of $[Ru(NH_3)_6]^{3+}$ absorbed on the surface of DNA. Differential pulse voltammetry (DPV) measurements were used to detect a series of TB standard solutions with different concentrations. As shown in Fig. 2A, as the TB concentration increased from 0 to 6 pM, the current value gradually increased. The DPV current value and the logarithm of the TB concentrations showed a good linear relationship (Fig. 2B). The corresponding linear equation was $I = 0.11555 \log C + 1.81296$ ($R^2 = 0.98$). According to the 3σ rule, a limit of detection (LOD) down to 0.1429 fM for TB was obtained (Fig. 2C). Compared with the analytical performance described in the previous literature on TB detection (Table 1), our aptasensor strategy had a lower detection limit. This result can be attributed to the TBA1–TB–TBA2 sandwich structure with a high load amount of $[Ru(NH_3)_6]^{3+}$.

Reproducibility, specificity and stability of the sensor

Three independent electrodes were individually used to measure 1 and 11 fM TB in parallel under the same conditions to test the repeatability of this electrochemical sensor (Fig. 3). The relative standard deviations (RSDs) of the three electrodes for 1 and 11 fM

Table 1 Comparison of the proposed assay and other reported techniques for the determination of TB

Method	Technique	Linear range	LOD	Ref.
Electrochemical	DPV	1 fM to 6 pM	0.1429 fM	This work
Electrochemical	DPV	5 pM to 5 nM	1.8 pM	30
Electrochemical	DPV	10 nM to 0.1 pM	25 fM	31
Electrochemical	DPV	0.5 pM to 30 nM	0.25 pM	32
Electrochemical	Chronoamperometry	0.1 pM to 20 nM	23 fM	33
Electrochemical	ACV[a]	10 pM to 100 nM	2.5 pM	34
Electrochemical	SWV[b]	0.05–100 nM	23.6 pM	5

[a] Alternating current voltammetry. [b] Square wave voltammetry.

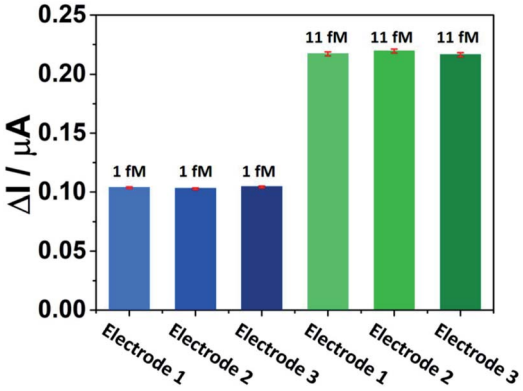

Fig. 3 The reproducibility assays of the three independent electrodes towards 1 and 11 fM TB in parallel under the same conditions.

TB were 0.08% and 0.17%, respectively, indicating that the aptasensor possessed an acceptable reproducibility. The specificity of the electrochemical sensor was also examined in the presence of various interfering substances, including Lys, Pep, Pap, Hem, BAS, and HAS. As shown in Fig. 4A, in contrast to the significant DPV signal of 10 fM TB, a negligible response was observed upon addition of all interferents with a concentration 100-fold higher than that of TB, testifying that the sensor had an excellent selectivity for TB. In addition, a very slight variation (RSD = 1.16%) was observed in the mixtures containing interfering substances (10 fM TB + 1 pM Hem, 10 fM TB + 1 pM BAS, and 10 fM TB + 1 pM HSA) and the target TB at 10 fM (Fig. 4B), also suggesting the outstanding selectivity of the sensor. In addition, the stability of the sensor was evaluated by storing it in a refrigerator at 4 °C. As shown in Fig. 5, after 43 h, the currents induced by 1 and 10 fM TB remained at 99.4% and 97% of the initial current values, and after 118 h, the initial DPV responses of 1 and 10 fM TB remained at 86.9% and 93.7%, revealing the excellent stability of the electrochemical sensor.

Human serum sample analysis

In order to prove the reliability of the aptasensor, the sensor was used to analyze TB in human serum samples. The serum samples were obtained from PLA General Hospital. Prior to

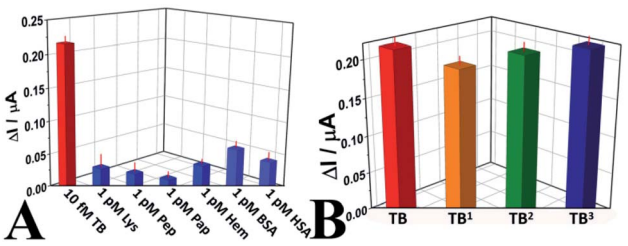

Fig. 4 (A) DPV signal from the electrochemical aptasensor in the presence of potential interferents, with a TB concentration of 10 fM, and Lys, Pep, Pap, Hem, BSA, and HSA concentrations of 1 pM. (B) Comparison of the DPV current response between 10 fM TB and the mixtures (TB^1: 10 fM TB + 1 pM Hem, TB^2: 10 fM TB + 1 pM BAS, and TB^3: 10 fM TB + 1 pM HSA).

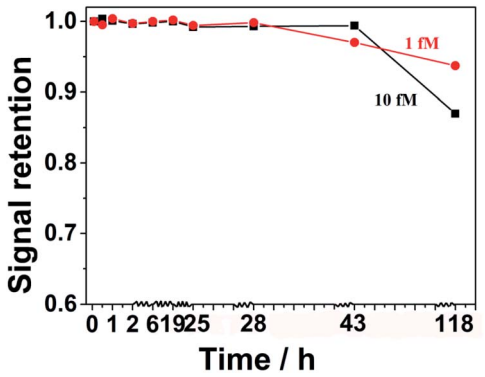

Fig. 5 The stabilization curve for the aptasensor.

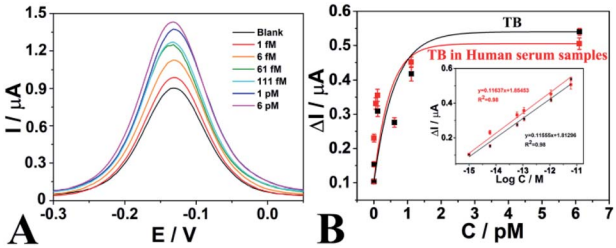

Fig. 6 (A) DPV responses of the electrochemical sensor towards different concentrations (0–6 pM) of TB in human serum samples. (B) Calibration curve for the current values of DPV and the different concentrations of TB in I–B buffer and human serum samples, respectively. Inset shows the corresponding linear relationship.

detection, we filtered the serum samples through 0.22 μm nitrocellulose membranes to remove physical impurities in the serum. Then, different concentrations of TB were spiked into the serum samples, respectively. The test procedure for TB in serum is the same as that in buffer solution. As shown in Fig. 6, compared with the TB standard curve in the I–B buffer solution, the actual standard curve for the sample was slightly higher, but the current value of DPV had a good linear relationship with the logarithm of the TB concentration (1 fM to 6 pM) in human serum samples, and the corresponding linear equation was $I = 0.11637 \log C + 1.85453$, with $R^2 = 0.98$, which shows that the sensor has a great potential for TB detection in actual samples.

Conclusions

In summary, we have developed an effective electrochemical aptasensor for ultrasensitive determination of TB based on TBA1–TB–TBA2 sandwich-type structure-triggered signal amplification. As AuNPs with a large specific surface area can bind numerous TBA2, more $[Ru(NH_3)_6]^{3+}$ can be adsorbed onto the TBA phosphate backbone when binding the target TB, resulting in a significant DPV current enhancement. The designed electrochemical sensor exhibited the advantages of a high sensitivity, selectivity, repeatability, and stability. The aptasensor showed a wide linear concentration range (1 fM to 6 pM) and a low detection limit (0.1429 fM) for TB. Most

importantly, the aptasensor could be used as a promising platform for the clinical detection of latent TB and has attractive prospects. This sensing strategy is expected to provide a promising solution for the detection of other proteins and biomolecules.

Conflicts of interest

There are no conflicts to declare.

Acknowledgements

All authors gratefully acknowledge financial support from the Scientific Research Project of Beijing Educational Committee (KM202010028007), and the Beijing Natural Science Foundation Program (2192010).

Notes and references

1 C. A. Holland, A. T. Henry, H. C. Whinna and F. C. Church, *FEBS Lett.*, 2000, **484**, 87.
2 Y. Wang and B. Liu, *Langmuir*, 2009, **25**, 12787.
3 J. Alzeer, B. R. Vummidi, P. J. C. Roth and N. W. Luedtke, *Angew. Chem., Int. Ed.*, 2009, **48**, 9362.
4 M. L. Nierodzik and S. Karpatkin, *Cancer Cell*, 2006, **10**, 355.
5 J. M. Yang, Y. L. Wu, C. F. Gan, R. Yuan and X. Yun, *Biosens. Bioelectron.*, 2018, **117**, 743.
6 P. P. Gai, C. C. Gu, H. Y. Li, X. Z. Sun and F. Li, *Anal. Chem.*, 2017, **89**, 12293.
7 J. F. Chang, X. Wang, J. Wang, H. Y. Li and F. Li, *Anal. Chem.*, 2019, **91**, 3604.
8 L. Ge, W. X. Wang, X. M. Sun, T. Hou and F. Li, *Anal. Chem.*, 2016, **88**, 9691.
9 G. Bayramoglu, V. C. Ozalp, M. Oztekin and Y. Arica, *Talanta*, 2019, **200**, 263.
10 G. Bayramoglu, V. Ozalp, U. Dincbal and Y. Arica, *ACS Biomater. Sci. Eng.*, 2018, **4**, 1437.
11 P. P. Gai, C. C. Gu, T. Hou and F. Li, *Anal. Chem.*, 2017, **89**, 2163.
12 G. Bayramoglu, C. Ozalp, M. Oztekin, U. Guler, B. Salih and M. Y. Arica, *Talanta*, 2019, **191**, 59.
13 W. Chen, C. Yan, L. Cheng, L. Yao, F. Xue and J. Xu, *Biosens. Bioelectron.*, 2018, **117**, 845.
14 L. Shi, X. Rong, Y. Wang, S. Ding and W. Tang, *Biosens. Bioelectron.*, 2018, **102**, 41.
15 Y. Xiao, A. A. Lubin, A. J. Heeger and K. W. Plaxco, *Angew. Chem., Int. Ed.*, 2005, **44**, 5456.
16 B. R. Baker, R. Y. Lai, M. S. Wood, E. H. Doctor, A. J. Heeger and K. W. Plaxco, *J. Am. Chem. Soc.*, 2006, **128**, 3138.
17 A. E. Radi, J. L. A. Sanchez, E. Baldrich and C. K. O'Sullivan, *J. Am. Chem. Soc.*, 2006, **128**, 117.
18 Y. Xiao, B. D. Piorek, K. W. Plaxco and A. J. Heeger, *J. Am. Chem. Soc.*, 2006, **127**, 17990.
19 X. L. Zuo, S. P. Song, J. Zhang, D. Pan, L. H. Wang and C. H. Fan, *J. Am. Chem. Soc.*, 2007, **129**, 1042.
20 X. H. Yin, T. Hou, B. Z. Huang, L. M. Yang and F. Li, *Chem. Commun.*, 2019, **55**, 13705.
21 Y. Zhang, H. H. Kim and A. Heller, *Anal. Chem.*, 2003, **75**, 3267.
22 S. Brakmann, *Angew. Chem., Int. Ed.*, 2004, **43**, 5730.
23 C. M. Niemeyer, *Angew. Chem., Int. Ed.*, 2001, **40**, 4128.
24 C. S. Thaxton, H. D. Hill, G. G. Dimitra, S. I. Stoeva and C. A. Mirkin, *Anal. Chem.*, 2005, **77**, 8174.
25 J. Zhang, S. Song, L. Zhang, L. Wang, H. Wu, D. Pan and C. H. Fan, *J. Am. Chem. Soc.*, 2006, **128**, 8575.
26 L. Shen, Z. Chen, Y. H. Li, S. L. He, S. B. Xie, X. D. Xu, Z. W. Liang, X. Meng, Q. Li, Z. W. Zhu, M. X. Li, X. C. Le and Y. H. Shao, *Anal. Chem.*, 2008, **80**, 6323.
27 K. C. Grabar, R. G. Freeman, M. B. Hommer and M. J. Natan, *Anal. Chem.*, 1995, **67**, 735.
28 R. Elghanian, J. J. Storhoff, R. C. Mucic, R. L. Letsinger and C. A. Mirkin, *Science*, 1997, **277**, 1078.
29 H. Z. Yu, C. Y. Luo, C. G. Sankar and D. Sen, *Anal. Chem.*, 2003, **75**, 3902.
30 C. Zhu, W. Zhu, L. Xu and X. Zhou, *Anal. Chim. Acta*, 2019, **1047**, 21.
31 B. He, *Microchim. Acta*, 2018, **185**, 344.
32 Q. Zhang, G. Fan, W. Chen, Q. Liu, X. Zhang, X. Zhang and Q. Liu, *Biosens. Bioelectron.*, 2020, **150**, 111846.
33 S. Chen, P. Liu, K. Su, X. Li, Z. Qin, W. Xu and J. Qiu, *Biosens. Bioelectron.*, 2018, **99**, 338.
34 Y. Ji, L. Zhang, L. Zhu, J. Lei, J. Wu and H. Ju, *Biosens. Bioelectron.*, 2017, **96**, 201.